Estimates of Beta Absorbed Fractions in Small Tissue Volumes for Selected Radionuclides

Gamal Akabani, John W. Poston, Sr., and Wesley E. Bolch

Nuclear Engineering Department, Texas A&M University, College Station, Texas

Energy deposition patterns are dependent upon the size and geometry of the source region, distribution of radioactive material, types of radiations and energies emitted by the radionuclide, as well as interfaces between different materials which may exist within the region. Commonly, in absorbed dose calculations for internally deposited beta-emitting radionuclides, it is assumed that the absorbed fraction of energy for the mean beta energy is a sufficient representation of the beta spectrum. The accuracy of this assumption was tested by comparing absorbed fractions calculated using actual beta spectral energies with those obtained using the mean beta energy for several radionuclides commonly used in nuclear medicine. A sphere composed of tissue was chosen as the preferred geometry. Spheres of 0.1, 0.5, 1.0, and 2.0 cm radius were used, and absorbed fractions were calculated as a function of surface-to-volume ratios. This allows the assessment of absorbed fraction in spheres where there is a uniform distribution of a radionuclide.

J Nucl Med 1991; 32:835–839

The importance of evaluating absorbed fractions of energy for small volumes is based on the need for better dosimetry associated with regions of the body that can be considered of special interest in nuclear medicine. These regions may be localized tumors or isolated regions which contain a known amount of radioactive material. Absorbed dose calculations for small volumes require the use of electron transport codes which are capable of evaluating their energy deposition patterns. Small volumes are considered in this paper to be regions which have a mean chord length from a fraction to several times the range of the maximum energy electron emitted by the radionuclide.

In this study, spheres of different radii were used in which a radionuclide was uniformly distributed. These spheres can be representative of many small regions and/or can be combined to provide an estimate of the absorbed dose to a specific region of the human body. The purpose of this paper is to report calculations of absorbed fractions of energy for spheres of different radii for selected radionuclides by using two methodologies. The first methodology considers the average energy of the beta spectrum to be representative of the radionuclide. The second method considers the entire beta spectrum. Given a specific radionuclide, results obtained from both methodologies are compared to assess their differences for any sphere size with a specific surface-to-volume ratio.

Received Jul. 17, 1990; revision accepted Oct. 22, 1990.

For reprints contact: Dr. Gamal Akabani, Dept. of Nuclear Engineering, Texas A&M University, College Station, TX 77843.

METHODOLOGY

Figure 1 shows a schematic representation of a tissue sphere of radius $2R_0$ subdivided into 100 concentric subregions or shells with thickness ΔR ($\Delta R = 2R_0/100$). The source region was defined analytically by a sphere of radius R_0. Monoenergetic electrons were generated uniformly and isotropically throughout the source region. Absorbed fractions for electron energies were calculated for every shell of the sphere. Six different spheres sizes were used and a complete set of electron absorbed fractions was generated for each sphere size. The radii (R_0) of the source regions of the tissue spheres were 2.0, 1.0, 0.5, 0.25, and 0.1 cm. The kinetic energies of the monoenergetic electrons were 0.05, 0.25, 0.5, 1.0, 1.5, 2.0, and 4.0 MeV. The absorbed fractions for zero kinetic energy represent the mathematical limit of the absorbed fractions; consequently, for shells inside the source region, the limiting absorbed fraction is given by the volume fraction of the source region. For regions outside the source region, the limiting absorbed fraction is zero.

To calculate the absorbed fractions of energy, the Monte Carlo code Electron-Gamma Shower (EGS4) was used in this research (*1*). The code is capable of simulating the transport of electrons and photons in any element, compound or mixture. In this research, the material in which electrons and photons were transported was tissue. The elemental composition of tissue was based on the data given by MIRD Pamphlet No. 5 Revised (*2*). The lower cutoff energies for electrons and photons were 10 keV and 1 keV, respectively. Photons or electrons with energies below these cutoffs were not transported and the remaining energy was assumed to be deposited locally.

The results obtained using the EGS4 code for monoenergetic electrons were used to calculate absorbed fractions of energy for actual spectra of various radionuclides. Information on radionuclides was obtained from the National Nuclear Data Center (Brookhaven National Laboratory) using the computer code RADLST (*3*). The spectra are given in the form of a histograms based on "group intensities." Each group intensity is given by the average energy of the "bin" corresponding to the width of each element of the histogram.

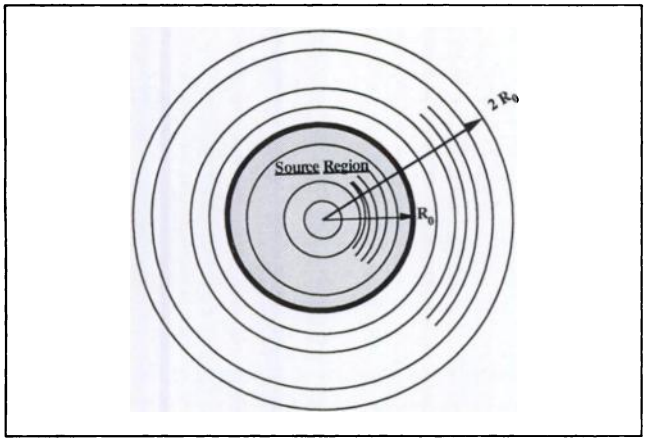

FIGURE 1. Schematic representation of a sphere used for calculation of absorbed fractions. The material is tissue and the sphere of radius $2R_0$ is subdivided into 100 concentric shells with thickness ΔR equal to $2R_0/100$. The source region is defined as a sphere of radius R_0.

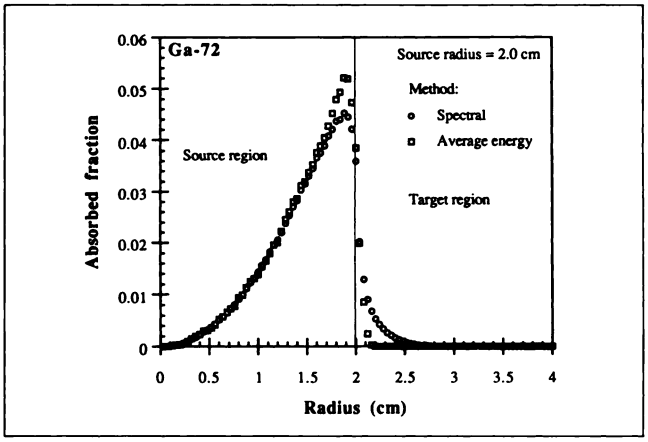

FIGURE 2. Absorbed fractions for the spherical shells as a function of their radii calculated for a 2.0 cm radius source region containing a uniform distribution of ^{72}Ga.

The energy deposited in each annular region of the sphere, ϵ_i, is calculated directly using the following equation:

$$\epsilon_i = \int_0^{T_{max}} T\frac{dI(T)}{dT}\phi(i,T)dT, \qquad \text{Eq. 1}$$

where dI(T)/dT is the differential energy probability distribution of the spectrum, T is the electron kinetic energy, and $\phi(i,T)$ is the absorbed fraction of energy in the i^{th} shell of the sphere. Equation 1 can be approximated by summing over energy groups:

$$\epsilon_i \cong \sum_j^n T_j I_j \phi_i, \qquad \text{Eq. 2}$$

where ϕ_i is the absorbed fraction for shell index i, and I_j is the group intensity at the mean energy T_j. The sum of the energy group decay intensities I_j is normalized to unity.

The average electron energy, $\overline{T}$, for a beta-decaying radionuclide is given by:

$$\overline{T} = \int_0^{T_{max}} T\,\frac{dI(T)}{dT}\,dT, \qquad \text{Eq. 3}$$

where Equation 3 can be approximated by

$$\overline{T} \approx \sum_j I_j T_j. \qquad \text{Eq. 4}$$

The absorbed fraction, ϕ_i, calculated by using the average electron energy, $\overline{T}$, is obtained by interpolating between the values of absorbed fractions for monoenergetic electrons; consequently, the absorbed fraction of the average electron energy is

$$\phi_i[\overline{T}] = \phi_i(\sum_j I_j T_j), \qquad \text{Eq. 5}$$

and the value of $\phi_i(\overline{T})$ must be calculated for every shell of the sphere to obtain an absorbed fraction profile. The energy deposited in the i^{th} shell under the above assumptions can be approximated by:

$$\epsilon_i = \overline{T}\phi_i(\overline{T}). \qquad \text{Eq. 6}$$

However, the energy deposited from the actual beta-decay spectra in the i^{th} shell is given in Equation 1. From Equation 1, *a weighted absorbed fraction* for a given radionuclide can be obtained by using the average energy to calculate the actual energy deposited in the i^{th} shell. The weighted absorbed fraction, $\overline{\phi}_i$, is then obtained by weighting the individual absorbed fractions of average group energies $\phi_i(T_j)$; i.e.,

$$\overline{\phi}_i = \frac{\sum_j I_j T_j \phi_i(T_j)}{\sum_j I_j T_j} \qquad \text{Eq. 7}$$

or

$$\overline{\phi}_i = \frac{\sum_j I_j T_j \phi_i(T_j)}{\overline{T}}. \qquad \text{Eq. 8}$$

By comparing $\overline{\phi}_i$ and $\phi_i(\overline{T})$, it is possible to assess the differences between the two methods for absorbed dose calculations.

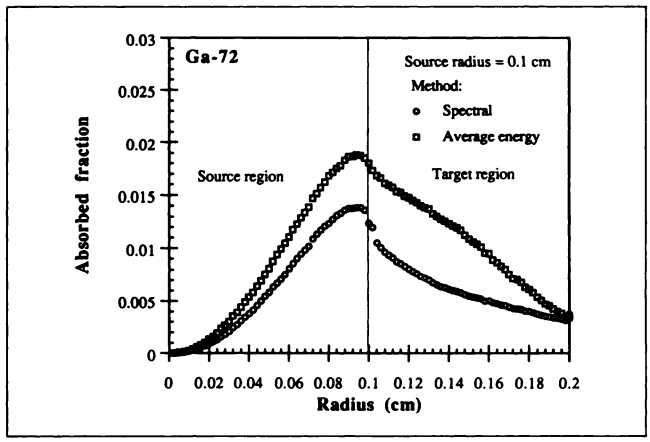

FIGURE 3. Absorbed fractions for the spherical shells as a function of their radii calculated for a 0.1 cm radius source region containing a uniform distribution of ^{72}Ga.

TABLE 1
Total Absorbed Fraction in the Source Region for Different Sphere Sizes Using Either the Emission Spectrum and Average Energy for Selected Radionuclides

	Sphere Size									
	0.1 cm		0.25 cm		0.05 cm		1.0		2.0 cm	
Radionuclide	a	b	a	b	a	b	a	b	a	b
^{133}Xe	0.89	0.95	0.96	0.98	0.98	0.99	0.99	1.00	0.99	1.00
^{99}Mo	0.43	0.60	0.71	0.83	0.85	0.91	0.93	0.96	0.96	0.98
^{111}In	0.82	0.94	0.93	0.98	0.96	0.99	0.98	0.99	0.99	1.00
^{114}In	0.22	0.23	0.49	0.59	0.71	0.79	0.85	0.89	0.92	0.94
^{11}C	0.50	0.62	0.77	0.84	0.88	0.92	0.94	0.96	0.97	0.98
^{120}Xe	0.52	0.60	0.78	0.83	0.89	0.91	0.94	0.96	0.97	0.98
^{121}Xe	0.13	0.10	0.33	0.37	0.57	0.64	0.77	0.81	0.88	0.90
^{123}Xe	0.28	0.30	0.59	0.66	0.78	0.82	0.89	0.91	0.94	0.95
^{124}I	0.20	0.18	0.45	0.53	0.67	0.75	0.83	0.88	0.91	0.93
^{125}Xe	0.85	1.00	0.94	1.00	0.97	1.00	0.98	1.00	0.99	1.00
^{126}I	0.40	0.48	0.70	0.77	0.84	0.88	0.92	0.94	0.96	0.97
^{129}I	0.97	0.99	0.99	0.99	0.99	1.00	1.00	1.00	1.00	1.00
^{130}I	0.56	0.73	0.79	0.89	0.89	0.94	0.95	0.97	0.97	0.99
^{131}I	0.73	0.86	0.89	0.94	0.94	0.97	0.97	0.99	0.98	0.99
^{13}N	0.39	0.46	0.69	0.76	0.84	0.88	0.92	0.94	0.96	0.97
^{14}C	0.97	0.98	0.99	0.99	0.99	1.00	1.00	1.00	1.00	1.00
^{18}F	0.68	0.78	0.86	0.91	0.93	0.95	0.97	0.98	0.98	0.99
^{15}O	0.24	0.27	0.53	0.63	0.74	0.81	0.87	0.90	0.93	0.95
^{24}Na	0.32	0.37	0.60	0.71	0.78	0.85	0.88	0.93	0.94	0.96
^{32}P	0.25	0.28	0.54	0.64	0.75	0.81	0.87	0.91	0.93	0.95
^{35}S	0.97	0.98	0.99	0.99	0.99	1.00	1.00	1.00	1.00	1.00
^{38}Cl	0.10	0.09	0.21	0.25	0.38	0.53	0.61	0.74	0.79	0.87
^{42}K	0.11	0.09	0.26	0.29	0.48	0.58	0.71	0.78	0.85	0.88
^{43}K	0.55	0.69	0.79	0.87	0.89	0.94	0.94	0.97	0.97	0.98
^{45}Ca	0.93	0.96	0.97	0.99	0.99	0.99	0.99	1.00	1.00	1.00
^{47}Sc	0.77	0.88	0.91	0.95	0.95	0.98	0.98	0.99	0.99	0.99
^{49}Ca	0.19	0.19	0.45	0.54	0.68	0.75	0.83	0.88	0.91	0.94
^{49}Sc	0.19	0.18	0.43	0.53	0.66	0.75	0.82	0.87	0.91	0.93
^{59}Fe	0.83	0.93	0.93	0.97	0.96	0.99	0.98	0.99	0.99	1.00
^{61}Co	0.39	0.50	0.69	0.79	0.83	0.89	0.92	0.95	0.96	0.97
^{66}Ga	0.08	0.07	0.18	0.20	0.37	0.45	0.62	0.70	0.80	0.84
^{72}Ga	0.33	0.45	0.55	0.76	0.72	0.88	0.85	0.94	0.92	0.97
^{73}Se	0.34	0.39	0.65	0.72	0.81	0.86	0.91	0.93	0.95	0.96
^{90}Sr	0.75	0.85	0.89	0.94	0.95	0.97	0.97	0.99	0.99	0.99
^{90}Y	0.17	0.16	0.39	0.48	0.63	0.72	0.80	0.86	0.90	0.93
^{99m}Tc	0.85	0.92	0.94	0.97	0.97	0.98	0.98	0.99	0.99	1.00

a = spectral method and b = average energy method.

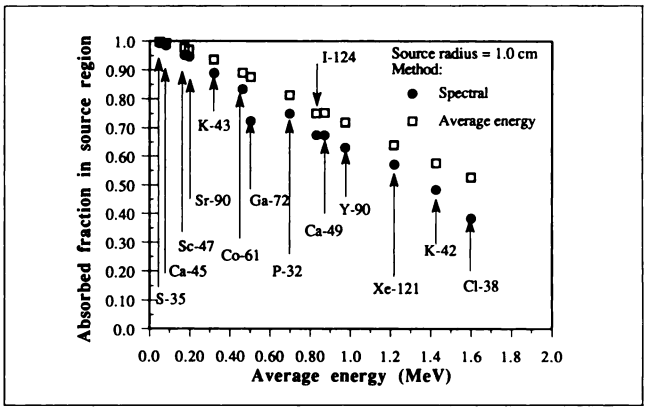

FIGURE 5. Absorbed fraction in the source region of a sphere of 1.0 cm radius for various radionuclides using average energy and spectral energies of the radionuclide.

RESULTS

Using the absorbed fractions for monoenergetic electrons and the spectra for selected radionuclides, absorbed fractions were calculated for specific radionuclides by using Equations 5 and 8 for the two methodologies, respectively. As an example, Figures 2 and 3 show the absorbed fraction profiles for ^{72}Ga for source regions with radii R_0 of 2.0 cm and 0.1 cm, respectively. The spectral profile is based on Equation 8 and the average energy profile is based on Equation 5.

Figure 2 shows that the use of the average energy of the spectrum provides an overestimate of the actual absorbed fraction in the source region when compared with that obtained using the entire beta spectrum. Conversely, the use of the average energy provides an underestimate of the total absorbed fraction outside the source region. Figure 3 shows that as the source volume decreases the differences between the two methodologies increase.

The total absorbed fraction in source region, ϕ_S, was evaluated by adding the individual absorbed fractions of

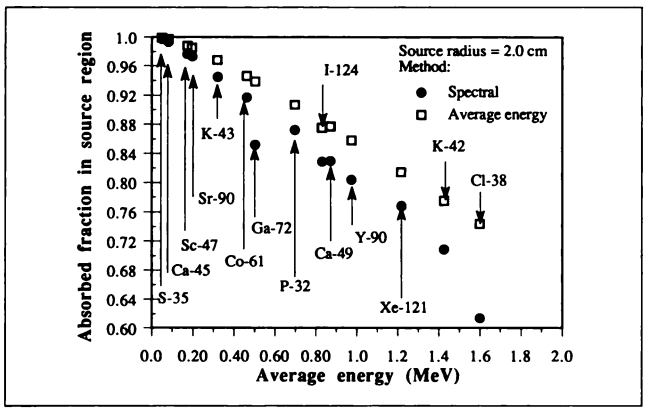

FIGURE 4. Absorbed fraction in the source region of a sphere of 2.0 cm radius for various radionuclides using average energy and spectral energies of the radionuclide.

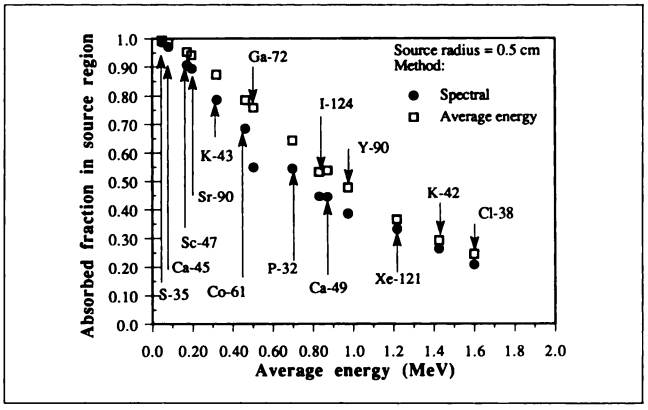

FIGURE 6. Absorbed fraction in the source region of a sphere of 0.5 cm radius for various radionuclides using average energy and spectral energies of the radionuclide.

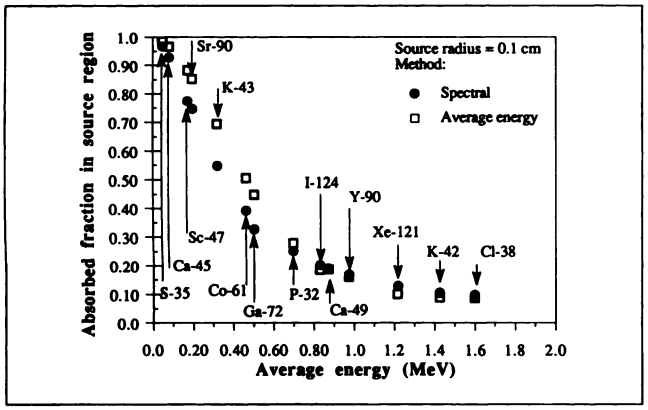

FIGURE 7. Absorbed fraction in the source region of a sphere of 0.1 cm radius for various radionuclides using average energy and spectral energies of the radionuclide.

shells inside source region (i = 1, 2, . . .50):

$$\phi_S = \sum_{i=1}^{50} \phi_i. \qquad \text{Eq. 9}$$

In the same manner, the total absorbed fraction in the target region, ϕ_T, was calculated for shells outside the source region (i = 51, 52, . . .100):

$$\phi_T = \sum_{i=51}^{100} \phi_i. \qquad \text{Eq. 10}$$

Table 1 presents a comparison of the total absorbed fractions for selected radionuclides in source regions of radii of 0.1, 0.5, 1.0, and 2.0 cm, respectively. Here, the absorbed fraction of energy obtained by using the average energy of the spectrum (Equation 5) is compared with the absorbed fraction obtained by considering the entire beta spectrum (Equation 8). Table 1 indicates clearly the importance of considering the beta spectrum as opposed to using the average beta energy in dosimetric calculations due to the differences in calculated absorbed fractions. The use of average energies generally leads to over-estimates of the absorbed fraction for the source regions; however, in cases where the source region becomes smaller, this relationship seems to reverse (for example ^{124}I and ^{49} Ca in Table 1). Therefore, the absorbed fraction is dependent on the spectral shape of the beta emitter.

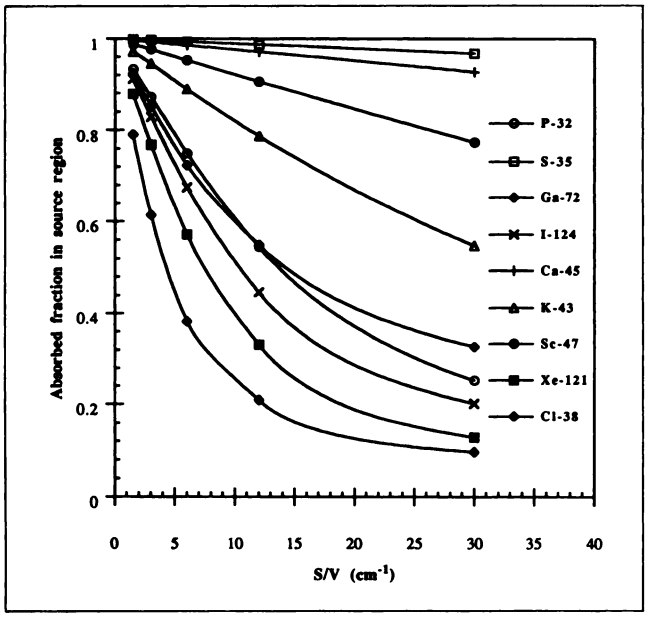

FIGURE 8. Absorbed fractions in the source region as a function of surface-to-volume ratios for various radionuclides.

Figures 4 through 7 show the total absorbed fraction in the source region, based on both methods, as a function of the radionuclide's average beta energy for spheres of different sizes. In these figures, the absorbed fraction values for a particular radionuclide are connected by a vertical line. This line is intended only to identify the pairs of data points and not to indicate the errors associated with the Monte Carlo calculations. From these figures, it is possible to approximately assess, under either methodology, the absorbed fractions of any radionuclide given its average beta energy.

Figure 8 shows another result of this study in which a relation between the surface-to-volume ratio and total absorbed fraction of energy in the source region is given for several radionuclides. Using these plots, or the data given in Table 1, an interpolation procedure can be applied to calculate the actual absorbed fraction for any spherical source region for various radionuclides by knowing the appropriate surface-to-volume ratio.

SUMMARY OF RESULTS

For volumes with radii on the order of several times the maximum electron range, the use of average electron energy of the beta spectrum gives a good approximation to the absorbed fraction when compared to results obtained using the emission spectrum of the radionuclide. When the volume of the source region becomes on the order of the range of the most energetic beta particle, the average energy electron absorbed fraction provides a conservative over-estimation of the actual absorbed fraction of energy. However, when the volume of the source region is a fraction of the range of the most energetic beta particle, the use of average electron energy can overestimate or underestimate the actual absorbed fraction depending on the softness or hardness of the emission spectrum of the radionuclide (e.g., ^{38}Cl, ^{121}Xe, ^{90}Y given in Table 1). The factors associated with the difference between both methods are the spectral shape and maximum electron energy of the radionuclide.

As stated above, Figure 8 shows absorbed fractions in the source region for various radionuclides as a function of surface-to-volume ratio. This plot can be used to obtain a relative estimate of absorbed fractions in the source region for any convex geometrical arrangement with a specific surface-to-volume ratio containing a specific radionuclide. The only restriction associated with this plot is

that the region must be convex and the radioactive material must be uniformly distributed in the source region.

ACKNOWLEDGMENTS

The authors would like to thank E.E. Watson, M.G. Stabin, R.J. Traub, and T.E. Hui for their helpful comments. This work was supported by grant DE-FG05-88ER60707 from the U.S. Department of Energy.

REFERENCES

1. Nelson WR, Hirayama H, Rogers DWO. The EGS4 code system. Stanford Linear Accelerator Center, Report 265, 1985.
2. Snyder WS, Ford MR, Warner GG. Estimates of specific absorbed fractions for photon sources uniformly distributed in various organs of a heterogeneous phantom. *MIRD pamphlet no. 5, revised.* New York: Society of Nuclear Medicine; 1978.
3. Burrows TW. The program RADLST. Brookhaven National Laboratory, New York, Information analysis center report, BNl-NCS-52142, 1988.

(continued from page 5A)

FIRST IMPRESSIONS

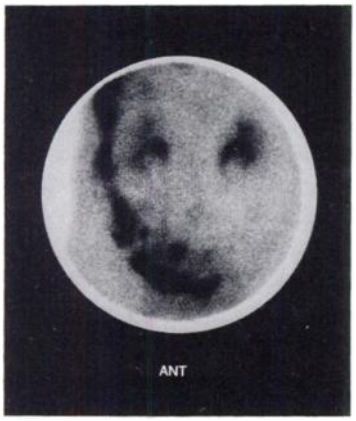

Figure 1

Figure 2

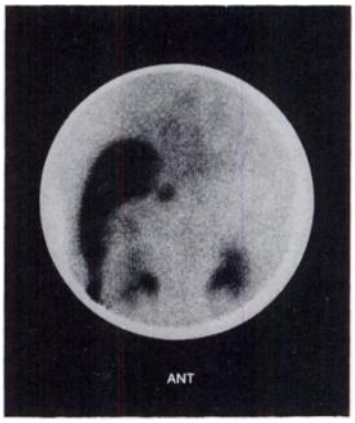

Figure 3

BACKGROUND:
Acute renal failure following prostatectomy. Technetium-99m-DTPA image at 30 min postinjection (Fig. 1).

PURPOSE:
A 64-yr-old male with benign prostatic hyperplasia was transferred to our institution two days after undergoing a suprapubic prostatectomy. His postoperative course was complicated by oliguria and acute renal impairment. An ultrasound documented normal renal size, morphology, and ascites. A combined ^{99m}Tc-DTPA and ^{131}I-hippuran renal scan was performed in order to confirm the clinical suspicion of a vesicoureteric leak. Anterior and right lateral DTPA images at 30 and 40 min, respectively, disclosed intact proximal ureters and renal pelves and radiolabeled urine in the peritoneal cavity in the perihepatic space, right pericolonic gutter, and lower abdomen (Figs. 2–3). Subsequent laparotomy confirmed inadvertent bilateral distal ureteric ligation and urinary leak.

TRACER:
15 mCi of ^{99m}Tc-DTPA and 200 μCi of ^{131}I

ROUTE OF ADMINISTRATION:
Intravenous

TIME AFTER INJECTION:
30–40 min (for ^{99m}Tc-DTPA images).

INSTRUMENTATION:
Siemens Orbiter (large field of view) with low-energy all-purpose collimator

CONTRIBUTORS:
G. Larcos and H.W. Wahner

INSTITUTION:
Department of Diagnostic Radiology, Section of Nuclear Medicine, Mayo Clinic and Mayo Foundation, Rochester, Minnesota